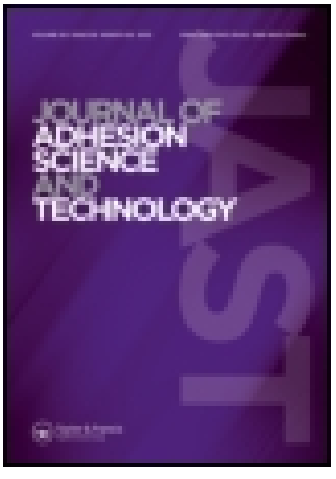

Journal of Adhesion Science and Technology
Publication details, including instructions for authors and subscription information:
http://www.tandfonline.com/loi/tast20

Prediction of combined effects of fibers and cement on the mechanical properties of sand using particle swarm optimization algorithm

Saman Soleimani Kutanaei[a] & Asskar Janalizadeh Choobbasti[a]
[a] Department of Civil Engineering, Babol University of Technology, P.O. Box 484, Babol, Iran
Published online: 02 Jan 2015.

To cite this article: Saman Soleimani Kutanaei & Asskar Janalizadeh Choobbasti (2015): Prediction of combined effects of fibers and cement on the mechanical properties of sand using particle swarm optimization algorithm, Journal of Adhesion Science and Technology, DOI: 10.1080/01694243.2014.995343

To link to this article: http://dx.doi.org/10.1080/01694243.2014.995343

Journal of Adhesion Science and Technology, 2014
http://dx.doi.org/10.1080/01694243.2014.995343

Prediction of combined effects of fibers and cement on the mechanical properties of sand using particle swarm optimization algorithm

Saman Soleimani Kutanaei* and Asskar Janalizadeh Choobbasti

Department of Civil Engineering, Babol University of Technology, P.O. Box 484, Babol, Iran

(*Received 17 October 2014; final version received 26 November 2014; accepted 1 December 2014*)

In this research, a series of laboratory tests have been performed to investigate the effects of cement and polyvinyl alcohol (PVA) fiber on the performance of sand. Unconfined compression strength and compaction are also assessed in the present study. The cement contents were 0.5, 1, 2, 4, and 6% by weight of the dry sand. Fiber length and diameter were 12 and 0.1 mm, respectively, and were added at 0.0, 0.3, 0.6, and 1% by weight of dry sand. Finally, the obtained results from the experimental data with particle swarm optimization algorithm are used to generate a polynomial model for prediction unconfined compression strength, modulus of elasticity, and axial strain at peak strength. The results of the study indicate that the inclusion of PVA fiber increases the unconfined compressive strength and the peak axial strain. The elastic modulus of specimen decreased with increase in fibers. Maximum dry density of the sand–cement–fiber mixture increases with the increase in cement content and decreases with the increase in fiber content.

Keywords: cement; fiber; UCS; compaction; sand

1. Introduction

In recent years, the number of suitable grounds for construction projects decreases with increasing population.[1,2] The soil existing in the sites may not suitable for construction from the engineering viewpoint and some changes should be applied to it in order to be prepared for such activities.[3,4] One of the appropriate solutions for encountering unsuitable soils in geotechnical engineering is change of soil properties, which is called ground improvement. Different improvement techniques such as using geomembranes, geotextiles, fibers, rice husk, cement, and lime can be used to increase shear strength parameters and bearing capacity of unstable soils.

Soil stabilization by adding materials such as cement, lime, bitumen, etc., is one of the effective methods for improving the geotechnical properties of soils which has been applied from many years ago. Cemented soils are generally used for the improvement of soft ground, the backfill materials of retaining walls, embankments, and for the subbase of roads and railroads, because cemented soils are less compressible and have an increased strength over that of natural soils. The mechanical behavior of cemented soils is influenced by a number of parameters including curing time, cement content, cement type, density, confining stress, grain size, and stress–strain history. According to the

*Corresponding author. Emails: samansoleimani16@yahoo.com, saman.soleimani@stu.nit.ac.ir

previous studies, the cementation can increase unconfined compressive strength (UCS), brittleness, shear strength, and dilative behavior of cement composites.[5,6]

The use of reinforcements in order to improve the behaviors of soils dates to ancient times. Several researchers have explored the effect of discrete randomly distributed fiber on mechanical properties of granular and clayey soils. These studies indicated that friction between fiber and soil particles can improve the ultimate and peak strength ductility of soils.[7–10] Yilmaz [11] conducted several laboratory split tensile and unconfined compression tests on sand–clay mixtures reinforced with polypropylene fibers. They found that the ratio of unconfined compression and split tensile strength of sand–clay mixtures significantly improved by fiber reinforcement. Liu [12] investigated the static liquefaction resistance of saturated sand reinforced with polypropylene fibers in undrained ring shear tests. The results showed that the inclusion of fiber significantly reduces the potential for the occurrence of liquefaction. Gao and Zhao [13] studied the effect of fiber orientations on the behavior of sand reinforced with fibers. The results showed that the fibers aligned to the horizontal direction in triaxial test will increase the shear strength parameters significantly. Shao et al. [14] investigated the shear strength of Jackson Mississippi sands reinforced with polypropylene fiber by carrying out a series of ring shear tests at different normal stresses. They reported that the inclusion of fiber had a significant effect on the shear strength parameters (cohesion and angle of internal friction) of the sand.

Some previous studies have been also reported on the influence of both randomly distributed fibers and cement on the mechanical properties of soils. The inclusions of cement into soil matrix result in a brittle behavior that can be controlled by the application of randomly distributed fibers.[15–19] Maher and Ho [20] carried out a large number of cyclic and static cyclic triaxial compression tests on cemented sand reinforced with randomly distributed discrete fibers. They found that the inclusion of fibers into cemented sand increased the energy absorption and shear strength. Tang et al. [21] have used polypropylene fiber and cement to improve the mechanical behavior clayey soil. They found that the fiber reinforcement causes an increase in shear strength parameters and unconfined compression strength. They also found that the discrete fibers prevent the development of cracks. Dos Santos et al. [22] performed a series of high-pressure triaxial compression tests in order to investigate the effect of fiber content on the hydrostatic compression behavior of cemented sand. Test results showed that the effects of the addition of fibers on the shear strength of cemented sand significantly depended on confining pressure. Consoli et al. [23] performed a large number of split tensile to the mechanical behavior of cemented soil reinforced with polypropylene fibers. The experimental results showed that the split tensile strength of cemented soil, over a wide cementation range, increased as fiber content increased. Estabragh et al. [24] conducted several unconfined compression tests to investigate the effect of nylon fiber on the mechanical behavior of cemented clay. They found that the inclusion of fibers within cemented clay caused an increase in the axial strain at failure and UCS, and changed the brittle behavior of the cemented clay to a more ductile behavior.

Nowadays, one of the most important parameters in many industrial procedures is optimization. Swarm intelligence methods (e.g. Particle swarm optimization algorithm (PSOA), genetic algorithm) are powerful tools for optimization of cost function. Among the available methods that can be applied to solve the engineering problems, PSO is proved to be intelligent, effective, robust and easy to apply. PSOA are population-based optimization algorithms inspired by animal social behavior such as bird and fish groups. Although, most previous investigations indicate that the PSOA is suitable

for geotechnical engineering applications.[25–28] Feng et al. [29] applied PSO algorithms for identification of the geotechnical parameters of viscoelastic constitutive models. Finsterle [30] presents the application of standard optimization algorithms for transport simulations of contamination plumes. Zhao and Yin [31] examined the potential use of PSOA for determination of geomechanical parameters. Choobbasti et al. [32] applied PSO techniques to optimize the position of the trench layer for the reduction of the liquefaction potential around a marine pipeline in porous seabed.

In this research, a series of laboratory tests have been performed to investigate the effects of cement and polyvinyl alcohol (PVA) fiber on the performance of sand. Unconfined compression strength and compaction are assessed in the present study. Finally, the obtained results from the experimental data with PSOA are used to generate a polynomial model for prediction unconfined compression strength, modulus of elasticity, and axial strain at peak strength.

2. Materials and specimen preparation

2.1. Sand

The sand used in this study was obtained from the coastal area of Caspian Sea in Babolsar, north of Iran. The soil is classified as poorly graded sand (SP) according to the unified soil classification system (USCS). The grain size distribution of the soil is shown in Figure 1. A scanning electron microscope (SEM) image of Khazar coastal sand with sub-rounded particles is shown in Figure 2(a). The index properties of the sand are presented in Table 1.

2.2. Cement

Ordinary Portland cement CEM I type with a strength class of 42.5 was used in this study. It was obtained from one of the cement companies in Iran. The chemical properties of cement are presented in Table 2.

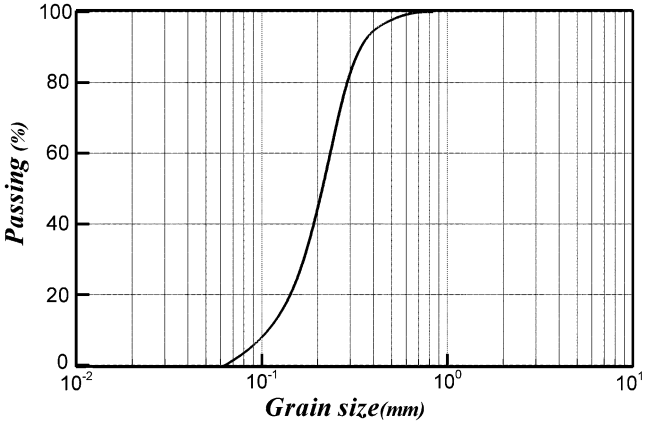

Figure 1. Particle size distribution.

Figure 2. (a) Scanning electron microscope (SEM) image of Khazar coastal sand, (b) Cement, and (c) PVA.

Table 1. Index properties of sand.

Parameter	Description	Value	Standard method
e_{max}	Maximum void ratio	0.8	ASTM D 4254
e_{min}	Minimum void ratio	0.526	ASTM D 4253
G_s	Specific gravity	2.78	ASTM D854
$C_u = D_{60}/D_{10}$	Coefficient of uniformity	2.128	–
$C_c = \left[D_{30}^2/(D_{60} \times D_{10})\right]$	Coefficient of gradation	1.322	–
D_{50}	Mean grain size of the sand (mm)	0.22	–
W_{opt}	Optimum moisture content (%)	16.1	ASTM D698
γ_d	Maximum dry density (kN/m^3)	16.9	ASTM D698
ϕ	Angle of internal friction (°)	38	ASTM D3080
c	Cohesion (kPa)	1	ASTM D3080

Table 2. Chemical properties of the cement.

Chemical name	Sio_2	Al_2o_3	Fe_2o_3	K_2o	Cao	Mgo	So_3	Nao_3
Percent (%)	21.25	21.25	3.19	0.63	64.07	1.20	2.04	3.08

2.3. *Fiber*

PVA (Figure 2(c)) fiber has been used in this research. The PVA fiber has 0.1 mm diameter and 12 mm length and its properties are shown in Table 3.

2.4. *Water*

Distilled water was used for sample preparation.

Table 3. Properties of PVA fiber.

Specific gravity	Cut length (mm)	Diameter (mm)	Tensile strength (MPa)	Young modulus (MPa)
1.3	12	0.1	1078	25,000

2.5. Specimen preparation

Dry sand and cement with a water content of 15% was mixed. Each portion of specimen was mixed by an electrical mixer with a predetermined amount of fiber to obtain a uniform fiber distribution. Cemented sand mixed with PVA fibers was compacted in five equal layers.[33] The cylindrical specimens had 38 mm diameter and 83 mm height. After compaction, the specimens were extruded from the mold and were kept in the humidity room at a constant temperature of 25 ± 2 °C. The cement content ρ_c and the fiber content ρ_f are defined as follows:

$$\rho_c = \frac{W_c}{W_s} \times 100\,(\%) \tag{1}$$

$$\rho_f = \frac{W_f}{W_s} \times 100\,(\%) \tag{2}$$

where W_s is the weight of dry sand, W_c is the weight of cement, and W_f is the weight of fiber.

3. Particle swarm optimization algorithm

PSOA was firstly introduced by Eberhart and Kennedy based on the population of particles.[34] Each particle is associated with velocity that indicates where the particle is traveling. If t be a time instant, the new particle position is computed by adding the velocity vector to the current position:

$$x^p(t+1) = x^p(t) + v^p(t+1) \tag{3}$$

being $x^p(t)$ particle p position, $p = 1,...,S$, at time instant t, $v^p(t+1)$ is the new velocity (at time $t+1$), and S is the population size. The velocity update equation is given by:

$$v_j^p(t+1) = \kappa 1 \cdot v_j^p(t) + \kappa 2 \cdot \omega_{1j}(t)\left(y_j^p(t) - x_j^p(t)\right) + \kappa 3 \cdot \omega_{2j}(t)\left(\hat{y}_j(t) - x_j^p(t)\right) \tag{4}$$

for $j = 1,...,n$, where $\kappa 1$ is a weighting factor (inertial), $\kappa 2$ is the cognitive parameter, and $\kappa 3$ is the social parameter that are set to 1, 1.5, and 2, respectively. ω_{1j} and $\omega_{2j}(t)$ are random numbers drawn from the uniform distribution (0,1), used for each dimension $j = 1,\ldots,\ n$. $y_j^p(t)$ is particle p position with the best objective function (goal function) value so far and $\hat{y}(t)$ is a particle position with the best function value so far.

Method can be described as follows:

(1) Randomly initialize the swarm positions, $X = \{x^1(0), \ldots, x^s(0)\}$ and velocities $V = \{v^1(0), \ldots, v^s(0)\}$
(2) Let $t = 0$ and $y^p(t) = x^p(t)$, $p = 1,...,\ s$.
(3) For all p in $\{1,...,\ s\}$ do:
    If $f(x^p(t)) < f(y^p(t))$, then set $y^p(t+1) = x^p(t)$ else set $y^p(t+1) = y^p(t)$.
(4) For all p in $\{1,...,\ s\}$ do:
(5) Compute $y^p(t+1)$ and $x^p(t+1)$, using Equations (3) and (4). If the stopping criterion is true, then stop. Otherwise, set $t = t+1$ goes to step 3. The structure of PSOA shows in Figure 3.

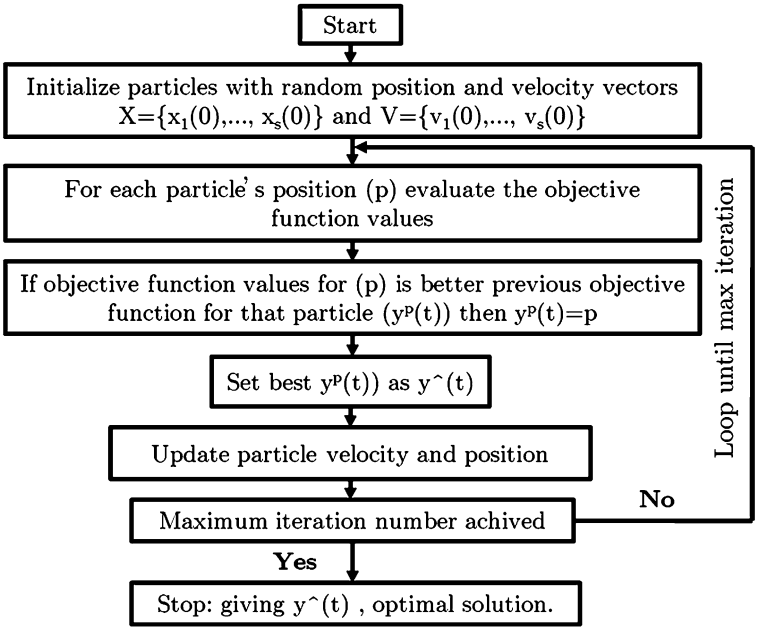

Figure 3. The standard elementary algorithm of PSOA.

4. Results and discussion

4.1. Compaction

Standard Proctor compaction tests were conducted in accordance with ASTM D698. The compaction process was done in three layers. Each layer was compacted with 25 blows. A series of standard Proctor tests were done for the soil samples containing 0, 2, 4, and 6% cement and 0, 0.3, 0.6, and 1% fiber by dry weight of soil.

Results on dry density vs. water content for sand, sand mixed with cement, and sand mixed with fiber are shown in Figure 4. As can be seen, maximum dry density of the sand–cement mixture increases with the increase in cement content. The increases in maximum dry density of sand mixed with cement for standard proctor compaction can be explained by two reasons. Cement has finer grains rather than sand; therefore, the void within the coarse aggregate becoming occupied by cement particles and make a dense and coherent structure with higher density. Cement has a higher specific gravity (3.1) than sand (2.78), which results in increasing the maximum dry unit weight when added to sand. The figure also reveals that there is decreasing trend in the optimum moisture content of the sand–cement mixture with the increase in cement content. But for all practical purposes, it can generally be concluded that the behavior of sand–cement mixes and sand is nearly similar.

Figure 4 also reveals that the maximum dry density of reinforced sand decreases with increasing fiber content. The interaction between soil particles and fiber restricts the movement of soil particles and causes a reduction in average unit weight of solids in the mixture of soil and fiber. The amount of fiber in sample has no effect on the optimum moisture content and the optimum moisture content does not show a significant change by the addition of fiber. More compaction energy appears necessary to produce specimens with higher fiber contents at a given dry density.

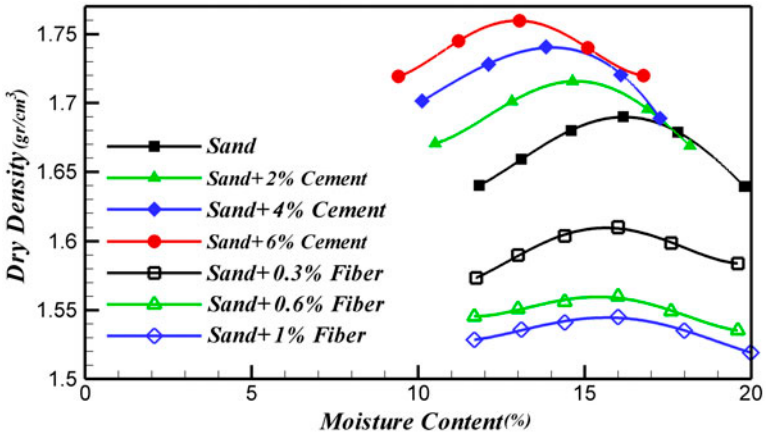

Figure 4. Standard compaction curve.

4.2. *Unconfined compression tests*

Unconfined compression tests were conducted in accordance with the ASTM D2166 test method. After curing, specimens were loaded at a displacement rate of 1 mm/min. Figure 5(a)–(c) represents typical results of unconfined compression tests conducted on unreinforced and reinforced specimen having 0.5 and 6% cement and 0, 0.3, 0.6, and 1% fiber. As can been seen in the figure, the stress–strain curves indicate a consistent increase in stress with strain up to a maximum peak stress value at which failure occurs. The value of the peak and the post-peak behavior are a function of the cement content and fiber content. The failure mode as indicated by the value of the strain at failure and by the post peak response is found to be more ductile as the fiber content increased from 0 to 1.0%.

The secant modulus of elasticity (E_{50}) was calculated from one-half of the axial strain at peak strength; straight lines were drawn up to 50% of axial compressive strength through the stress–strain curves; and the slope of these lines is taken as the secant modulus of elasticity (Figure 6(a)).

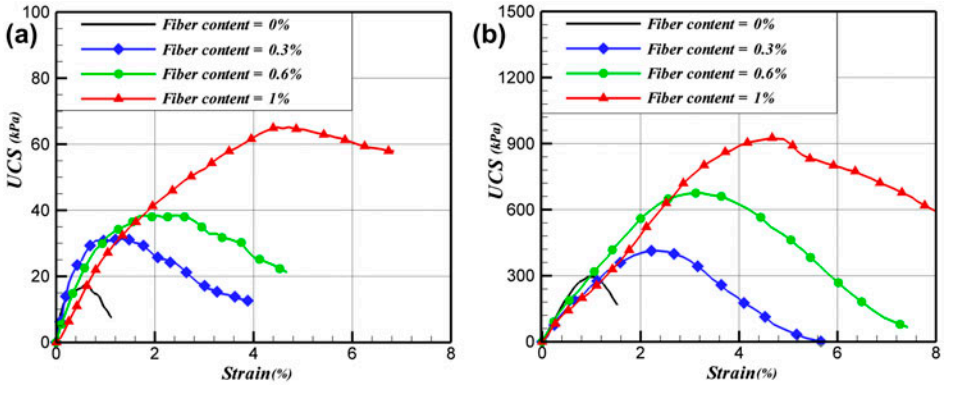

Figure 5. Stress–strain curve of specimen with 0, 0.3, 0.6, and 1% (a) 0.5% cement, (b) 6% cement.

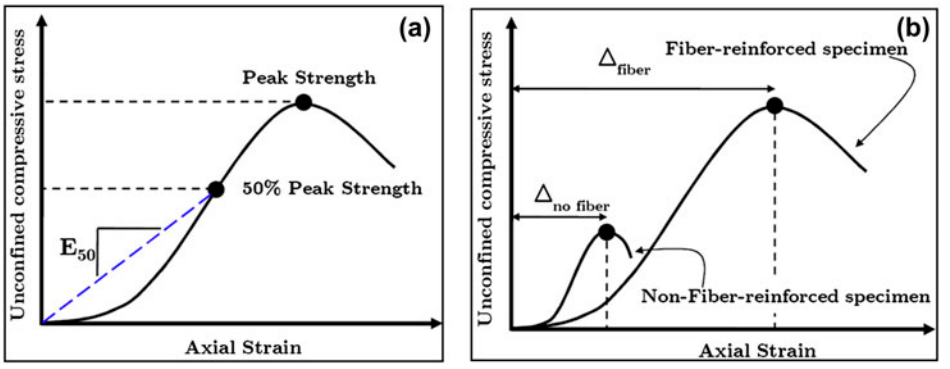

Figure 6. (a) Modulus of elasticity, E_{50}, (b) deformability index, D.

Park defined a strain-based index called the deformability index, which is the ratio of the axial strain at peak strength in fiber reinforcement specimen to the axial strain at peak strength in nonfiber-reinforced specimen. Deformability index is defined as follows [34]:

$$D = \frac{\Delta_{\text{fiber}}}{\Delta_{\text{no fiber}}} \tag{5}$$

where Δ_{fiber} is the axial strain at peak strength in fiber reinforcement specimen, and $\Delta_{\text{no fiber}}$ (Figure 6(b)) is the axial strain at peak strength in nonfiber-reinforced specimen.

The increase in the UCS due to the inclusion of PVA fiber is quantified by R in Equation (6).

$$R = \frac{\text{UCS}_{\text{fiber}}}{\text{UCS}_{\text{no fiber}}} \tag{6}$$

The summary of results from unconfined compression tests are presented in Table 4.

In the present study, an attempt has been made to develop empirical relationships to estimate the UCS, axial strain at peak strength, secant modulus of elasticity as functions of cement, and fiber content. Using PSOA, the following polynomial model for UCS, axial strain at peak strength, and secant modulus of elasticity is obtained:

$$\text{UCS},\ E_{50},\ \varepsilon_a = a_1 + a_2\rho_c + a_3\rho_f + a_4{\rho_c}^2 + a_5\rho_c\rho_f + a_6{\rho_f}^2 \tag{7}$$

Evaluation and validation of a_i coefficients in the polynomial model constitutes the main goal of PSOA. The coefficient for Equation (7) is present in Table 5.

Figure 7 shows the result obtained by PSOA for different iteration numbers. The figure shows the random initial position of the particles (0 iteration) and particle movement during the solution procedure for estimated value of UCS, as well as it demonstrates that most of the particles approach the best objective function value by 40 iterations.

Figure 8 shows regression value obtained between result of polynomial model and available experimental data for prediction of unconfined compression strength and axial strain at peak strength. The regression value is 0.987 and 0.995 for unconfined compression strength and axial strain at peak strength, respectively, which shows that the polynomial model is able to predict the outputs successfully.

Table 4. Summary of unconfined compression tests.

Specimen	Cement ratio (%)	Fiber ratio (%)	UCS (%)	Axial strain at peak strength (%)	R	D	E_{50}
A-0	0.5	0	15	0.81	1	1	2.9
A-1	0.5	0.3	30	1.79	1.9	2.2	2.5
A-2	0.5	0.6	43	2.8	2.7	3.4	2.0
A-3	0.5	1	65	4.71	4.0	5.8	1.8
B-0	1	0	51	1.02	1	1	5.9
B-1	1	0.3	87	1.95	1.7	1.9	5.3
B-2	1	0.6	134	2.97	2.6	2.9	4.5
B-3	1	1	197	4.53	3.8	4.4	3.4
C-0	2	0	171	1.17	1	1	19.1
C-1	2	0.3	254	2.19	1.4	1.8	15.3
C-2	2	0.6	444	3.21	2.5	2.7	13.8
C-3	2	1	632	4.58	3.6	3.9	12.3
D-0	4	0	309	1.19	1	1	38.5
D-1	4	0.3	439	2.38	1.4	2	29.4
D-2	4	0.6	687	3.29	2.2	2.7	27.4
D-3	4	1	915	4.96	2.9	4.1	23.1
E-0	6	0	476	1.18	1	1	46.1
E-1	6	0.3	642	2.25	1.3	1.9	39.6
E-2	6	0.6	809	3.37	1.6	2.8	36.5
E-3	6	1	1237	5.28	2.5	4.4	34.3

Table 5. Coefficient to estimate the UCS, E_{50}, and ε_a.

	a_1	a_2	a_3	a_4	a_5	a_6
UCS	−95.357	173.89	55.516	15.055	125.16	126.7
E_{50}	−2.375	11.469	7.7406	0.54483	2.1674	6.3156
ε_a	0.82801	0.17346	2.8949	0.018129	0.068555	0.63372

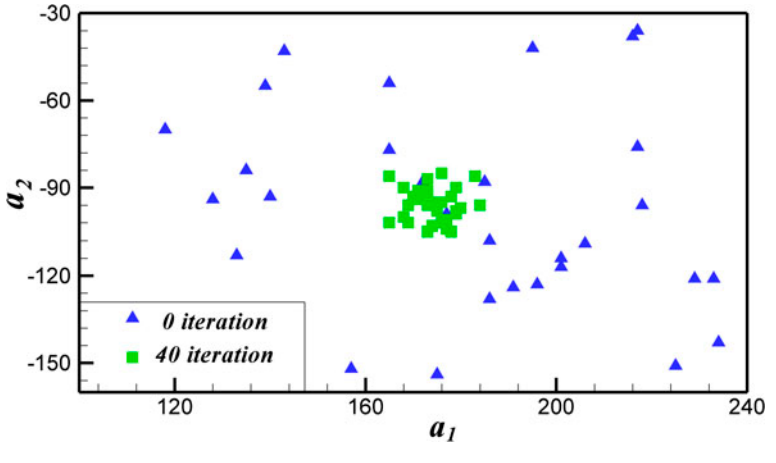

Figure 7. Particles movement during the solution procedure.

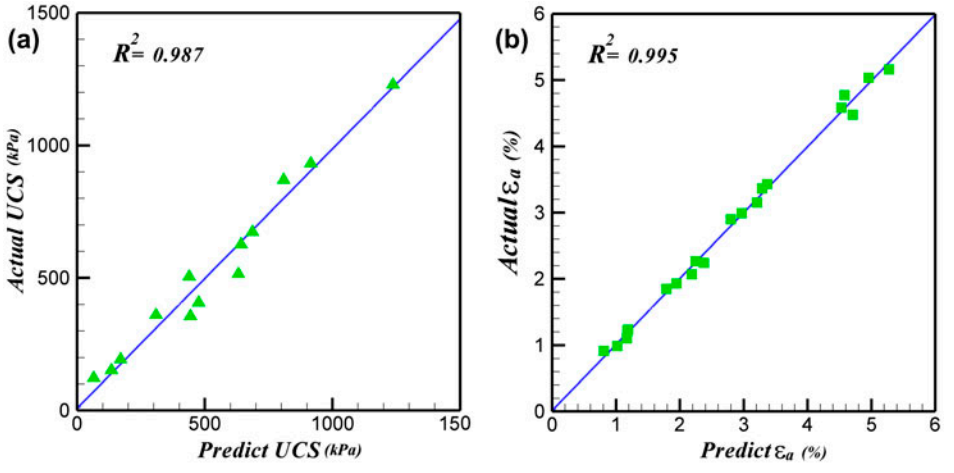

Figure 8. Performance of polynomial model in terms of regression value.

Figure 9 shows the variation of UCS with fiber and cement content. Figure 9 revels that the UCS is proportional to the fiber content and cement content. As the fiber ratio increases, the UCS of fiber-reinforced cemented sand increases to more than four times that of the unreinforced cemented sample. The same trend for UCS with other types of fiber was reported by several researchers. For unreinforced samples, the increase in cement content from 0.5 to 6% increased the UCS from 15 to 476 kPa.

As shown in Table 4, the increase in the values of R decreases with increasing cement content. This result revels that for lower cement content, the inclusion of fiber has a higher impact in UCS compared with a sample of bigger cement content. This may be attributed to the fact that the tensile strength of the randomly distributed discrete fibers would be mobilized only after deformation of the sand particles around the

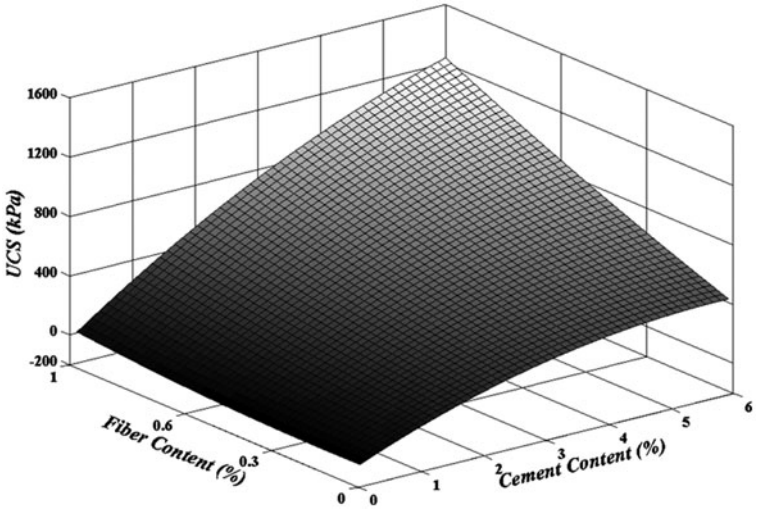

Figure 9. Variation of UCS with fiber and cement content.

fibers. The portion of UCS to be mobilized significantly depends on the magnitude of the sand particles deformation and also on the stiffness of the fibers. The fiber-reinforced cemented sand stiffness and strength increase with increasing cement content. For high cement contents, the amount of cement content. It can be expected that for high cement content, reinforcing elements due to being less stiff are not able to mobilize shear strength, because low deformation occurs between sand particles and fibers. The similar observations were reported by a number of researchers. Maher and Ho mixed 4% cemented and 1% glass fiber with Ottawa sand. They found that R was approximately 1.5.[20] Kumar et al. mixed clay with 10% sand and 1% polyester fiber and found that R was approximately 1.2.[35] Maher and Ho tested a specimen of 1% Polypropylene fiber and 1% glass fiber that was mixed with Kaolinite clay, and found that R was approximately 1.2.[36]

The effect of fiber and cement content on axial strain at peak strength is shown in Figure 10. It can be seen that the axial strain at failure increases with increasing fiber content. The results reveal that inclusion of randomly distributed fibers delays failure and improves the brittle behavior. The figure also indicates that when the fiber content is constant, the axial strain at failure is almost the same, regardless of the cement content. As shown in Table 4, the deformability index increase with increasing fiber content. UCS of cemented soils increases with increasing cement content; this causes a brittle or sudden failure without plastic deformation. As the confining pressure increases, the brittle behavior of cemented sand changes to a more ductile behavior. In particular, when applying cemented sand at a shallow depth, the degree of brittle behavior may be more pronounced due to a low confining pressure.

Figure 11 shows the variation of modulus of elasticity with fiber content with different cements. As shown in this figure, the inclusion of fibers into samples reduces the secant modulus of elasticity. This behavior may be explained by the fact that extensible randomly distributed fibers require an initial deformation to begin tensile strength mobilization that results in the reduction of sample stiffness. Past literature shows that an increase in the fiber content in reinforced sample has the same effect as an increase in the

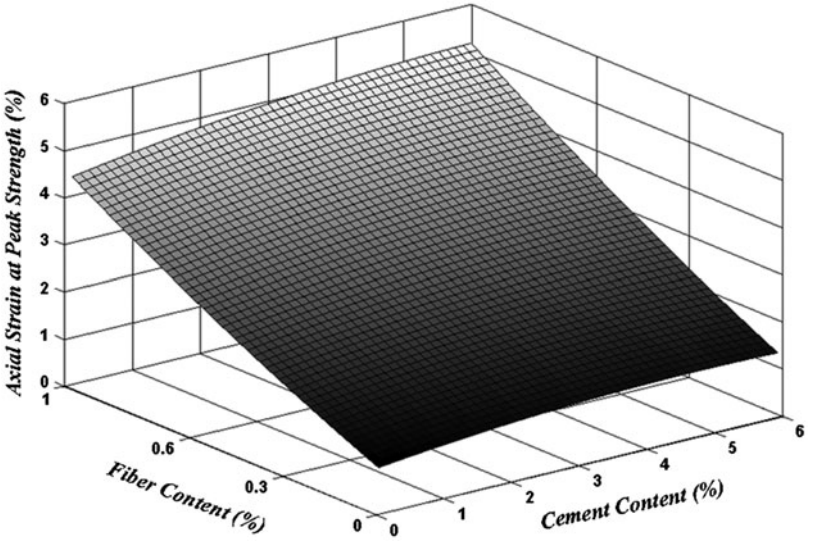

Figure 10. Variation of axial strain at peak strength with fiber and cement.

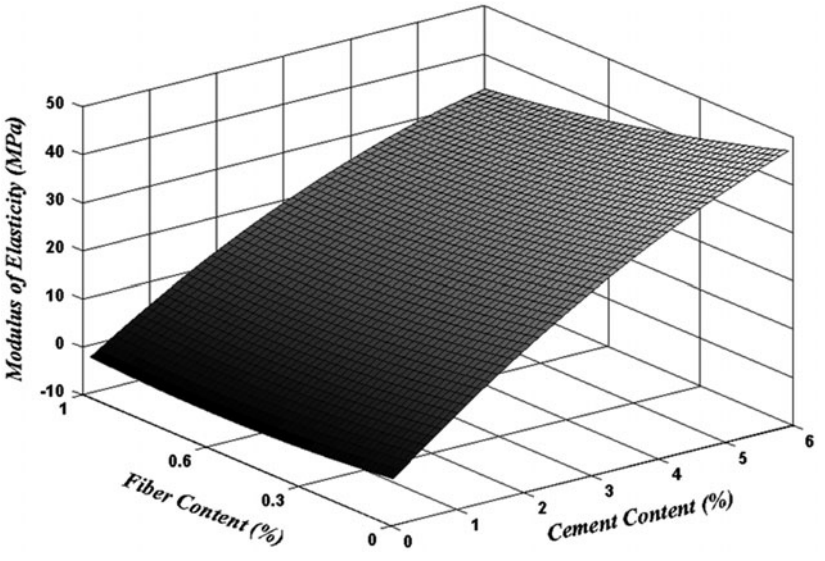

Figure 11. Variation of modulus of elasticity with fiber and cement.

confining pressure in unreinforced sample in the triaxial test.[37–39] Past studies show that the horizontal deformation of sample decreases with an increase in confining pressure. The horizontal deformation of fiber-reinforced sample was also restrained by the increase in the fiber content. Yang reports that the increase in peak deviatoric stress in the fiber-reinforced sample was attributable to the increase in the confining pressure.[39]

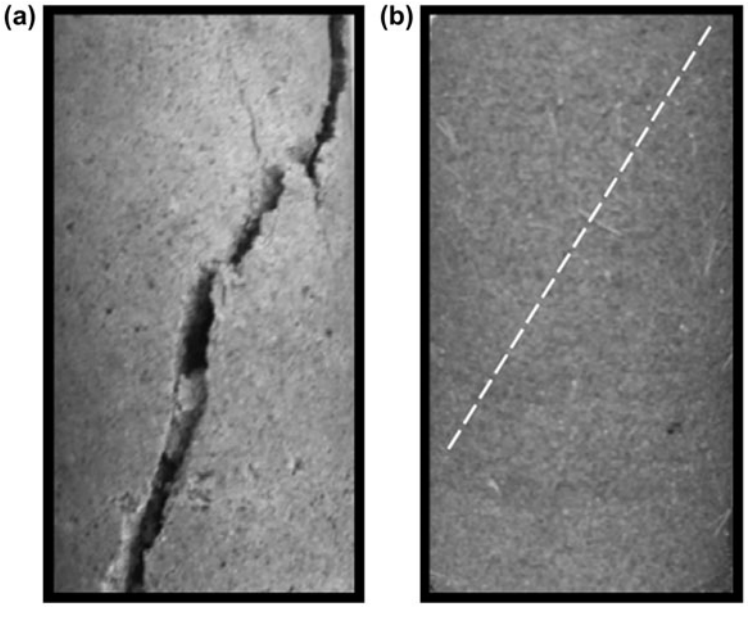

Figure 12. Specimen with 6% cement content after failure (a) 0% fiber, (b) 1% fiber.

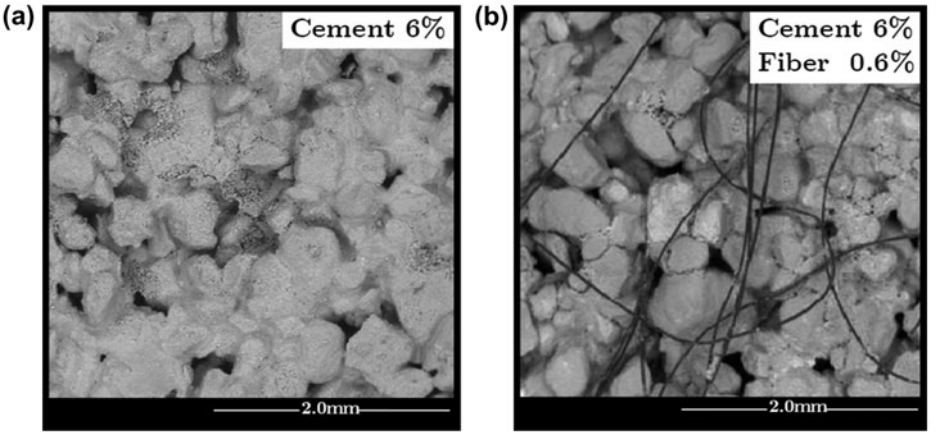

Figure 13. SEM image (a) cemented specimens with cement content of 6%, (b) fiber-reinforced cemented sand with 6% cement and 0.6% fiber.

Figure 12 shows photographs of the unreinforced cemented sample and reinforced cemented sample after failure. In the unreinforced sample, a crack throughout the entire specimen appeared after failure, as shown in Figure 12(a). The failure of the fiber-reinforced cemented specimen occurred due to slippage between the sand particles and the fibers (Figure 12(b)). Inclusion of fiber to cemented sand produces strong frictional interaction between the fibers and the soil particles and reduces the brittle behavior of cemented sand

Scanning electron microscopy (SEM) was used to analyze the homogeneity of the sample before testing. Typical SEM photos obtained from cutup sections of cemented samples with 6% cement and fiber-reinforced cemented sample with 0.6% fiber and 6% cement are shown in Figure 13(a) and (b), respectively. The SEM photos were taken after curing. It can be observed from the figure that in the samples, the sand particles are well coated by the cement. Figure 13 indicates that for fiber-reinforced sample, although prior to the sample preparation, the mixing was continued until achieving a uniform fiber distribution throughout the entire sample; however, the SEM photos from the sample indicate that at microscale, the homogeneity and uniformity are not as good as observed in the visual inspection.

4.3. Matric suction measurement.

The matric suction tests were conducted in accordance with the accordance with ASTM D5298 using the filter paper technique (Whatman No. 42) after failure in the unconfined compression tests. Its initial moisture content, in the air dried condition, is approximately 5.5%, which allows measurements of suction from zero to 28 MPa. The calibration equations for this filter paper are presented by Chandler et al. [40].

5. Conclusion

This research evaluated the combined effects of cement and fibers on the mechanical properties and compaction characters of sand. Particle swarm optimization method is utilized for evaluation of the coefficient of polynomial model for prediction of UCS,

axial strain at peak strength, and secant modulus of elasticity. The results of this study can be summarized as follow:

(1) Comparison shows that the polynomial model obtained from PSOA has good agreement with experimental results.
(2) The addition of cement to the sand significantly increased the modulus of elasticity and unconfined compression strength and changed the sand behavior to a noticeably more brittle behavior.
(3) The addition of fiber to the cemented sand decreased the modulus of elasticity.
(4) Inclusion of fiber causes an increase in unconfined compression strength in the cemented sand. Moreover, deformability index significantly increases with increasing fiber content. At low fiber content ($\rho_c < 1\%$), deformability index was not influenced by the cement content.
(5) Due to the ductile behavior of the fiber reinforced cemented sand, the axial strain at failure of samples with 6% cement content increases up to 5% as the fiber content increases.

References

[1] Tavakoli HR, Kutanaei SS. Evaluation of effect of soil characteristics on the seismic amplification factor using the neural network and reliability concept. Arab. J. Geosci. doi:10.1007/s12517-014-1458-z.
[2] Sarokolayi LK, Beitollahi A, Abdollahzadeh G, Amreie ST, Kutanaei SS. Modeling of ground motion rotational components for near-fault and far-fault earthquake according to soil type. Arab. J. Geosci. doi:10.1007/s12517-014-1409-8.
[3] Rezaei S, Choobbasti AJ, Kutanaei SS. Site effect assessment using microtremor measurement, equivalent linear method, and artificial neural network (case study: Babol, Iran). Arab. J. Geosci. doi:10.1007/s12517-013-1201-1.
[4] Janalizadeh A, Kutanaei SS, Ghasemi E. CVFEM modeling of free convection inside an inclined porous enclosure with a sinusoidal hot wall. Sci. Iran. A. 2013;20:1401–1414.
[5] Tavakoli HR, Omran OL, Shiade MF, Kutanaei SS. Prediction of combined effects of fibers and nanosilica on the mechanical properties of self-compacting concrete using artificial neural network. Lat. Am. J. Solids Struct. 2014;11:1906–1923.
[6] Tavakoli HR, Omran OL, Kutanaei SS, Shiade MF. Prediction of energy absorption capability in fiber reinforced self-compacting concrete containing nano-silica particles using artificial neural network. Lat. Am. J. Solids Struct. 2014;11:966–979.
[7] Babu GLS, Chouksey SK. Stress–strain response of plastic waste mixed soil. Waste Manage. 2011;31:481–488.
[8] Kumar A, Walia BS, Mohan J. Compressive strength of fiber reinforced highly compressible clay. Constr. Build. Mater. 2006;20:1063–1068.
[9] Kaniraj SR, Havanagi VG. Behavior of cement-stabilized fiber-reinforced fly ash-soil mixtures. J. Geotech. Eng. Div. 2001;127:574–584.
[10] Consoli NC, Festugato L, Heineck KS. Strain-hardening behaviour of fibre-reinforced sand in view of filament geometry. Geosynth. Int. 2009;16:109–115.
[11] Yilmaz Y. Experimental investigation of the strength properties of sand–clay mixtures reinforced with randomly distributed discrete polypropylene fibers. Geosynth. Int. 2009;16:354–363.
[12] Liu J, Wang G, Kamai T, Zhang F, Yang J, Shi B. Static liquefaction behavior of saturated fiber-reinforced sand in undrained ring shear tests. Can. Geotech. J. 2011;29:462–471.
[13] Gao Z, Zhao J. Evaluation on failure of fiber-reinforced sand. J. Geotech. Geoenviron. 2013;139:95–106.
[14] Shao W, Cetin B, Li Y, Li J, Li L. Experimental investigation of mechanical properties of sands reinforced with discrete randomly distributed fiber. Geotech. Geol. Eng. 2014;32:901–910.
[15] Consoli NC, Montardo JP, Donato M, Prietto PDM. Effect of material properties on the behaviour of sand–cement–fibre composites. Ground Improv. 2004;8:77–90.

[16] Consoli NC, Vendruscolo MA, Fonini A, Dalla Rosa F. Fiber reinforcement effects on sand considering a wide cementation range. Geotext. Geomembr. 2009;27:196–203.
[17] Consoli NC, Bassani MAA, Festugato L. Effect of fiber-reinforcement on the strength of cemented soils. Geotext. Geomembr. 2010;28:344–351.
[18] Consoli NC, Vendruscolo MA, Prietto PDM. Behavior of plate load tests on soil layers improved with cement and fiber. J. Geotech. Eng. Div. 2003;129:96–101.
[19] Onishi K, Tsukamoto Y, Saito R, Chiyoda T. Strength and small-strain modulus of light-weight geomaterials: cement-stabilised sand mixed with compressible expanded polystyrene beads. Geosynth. Int. 2010;17:380–388.
[20] Maher MH, Ho YC. Behavior of fiber-reinforced cemented sand under static and cyclic loads. Geotech. Test. J. 1993;16:330–338.
[21] Tang C, Shi B, Gao W, Chen F, Cai Y. Strength and mechanical behavior of short polypropylene fiber reinforced and cement stabilized clayey soil. Geotext. Geomembr. 2007;25:194–202.
[22] Dos Santos APS, Consoli NC, Heineck KS, Coop MR. High-pressure isotropic compression tests on fiber-reinforced cemented sand. J. Geotech. Eng. Div. 2010;136:885–890.
[23] Consoli NC, Zortéa F, de Souza M, Festugato L. Studies on the dosage of fiber-reinforced cemented soils. J. Mater. Civ. Eng. 2011;23:1624–1632.
[24] Estabragh AR, Namdar P, Javadi AA. Behavior of cement-stabilized clay reinforced with nylon fiber. Geosynth. Int. 2012;19:85–92.
[25] Soleimani S, Ganji DD, Gorji M, Bararnia H, Ghasemi E. Optimal location of a pair heat source-sink in an enclosed square cavity with natural convection through PSO algorithm. Int. Commun. Heat Mass. 2011;38:652–658.
[26] Yuan S, Wang S, Tian N. Swarm intelligence optimization and its application in geophysical data inversion. Appl. Geophys. 2009;6:166–174.
[27] Song X, Tang L, Lv Xiaochun, Fang H, Gu H. Application of particle swarm optimization to interpret Rayleigh wave dispersion curves. J. Appl. Geophys. 2012;84:1–13.
[28] Kutanaei SS, Roshan N, Vosoughi A, Saghafi S, Barari A, Soleimani S. Numerical solution of stokes flow in a circular cavity using mesh-free local RBF-DQ. Eng. Anal. Boundary Elem. 2012;36:633–638.
[29] Feng XT, Chen BR, Yang C, Zhou H, Ding X. Identification of visco-elastic models for rocks using genetic programming coupled with the modified particle swarm optimization algorithm. Int. J. Rock Mech. Min. Sci. 2006;43:789–801.
[30] Finsterle S. Demonstration of optimization techniques for groundwater plume remediation using iTOUGH2. Environ. Modell. Software. 2006;21:665–680.
[31] Zhao H, Yin S. Geomechanical parameters identification by particle swarm optimization and support vector machine. Appl. Math. Modell. 2009;33:3997–4012.
[32] Choobbasti AJ, Tavakoli H, Kutanaei SS. Modeling and optimization of a trench layer location around a pipeline using artificial neural networks and particle swarm optimization algorithm. Tunn. Undergr. Sp. Tech. 2014;40:192–202.
[33] Park SS. Effect of fiber reinforcement and distribution on unconfined compressive strength of fiber-reinforced cemented sand. Geotext. Geomembr. 2009;27:162–166.
[34] Eberhart R, Kennedy J. New optimizers using particle swarm theory. In: Proceedings of the 6th International Sysmposium on Micro Machine and Human Science; Nagoya; 1995. p. 39–43.
[35] Kumar A, Walia BS, Mohan J. Compressive strength of fiber reinforced highly compressible clay. Constr. Build Mater. 2006;20:1063–1068.
[36] Maher MH, Ho YC. Mechanical properties of kaolinite/fiber soil composite. J. Geotech. Eng. 1994;120:1381–1393.
[37] Abdulla AA, Kiousis PD. Behavior of cemented sands—I. Testing. Int. J. Numer. Anal. Methods Geomech. 1997;21:533–547.
[38] Clough GW, Sitar N, Bachus RC, Rad NS. Cemented sands under static loading. J. Geotech. Eng. Div. 1981;107:799–817.
[39] Yang Z. Strength and deformation characteristics of reinforced sand [PhD thesis]. Los Angeles (CA): University of California; 1972.
[40] Chandler RJ, Crilly MS, Montgomery-Smith G. A low-cost method of assessing clay desiccation for low-rise buildings. In: Proceedings of the Institute of Civil Engineers, London. 1992;2:82–89.